Monthly Notices
of the
ROYAL ASTRONOMICAL SOCIETY

MNRAS **493,** L16–L21 (2020) doi:10.1093/mnrasl/slz187

The pancaking of coronal mass ejections: an *in situ* attestation

Anil N. Raghav [1]★ and Zubair I. Shaikh [2]

[1] *University Department of Physics, University of Mumbai, Vidyanagari, Santacruz (E), Mumbai 400098, India*
[2] *Indian Institute of Geomagnetism (IIG), New Panvel, Navi Mumbai 410218, India*

Accepted 2019 December 17. Received 2019 December 17; in original form 2019 September 24

ABSTRACT

The interplanetary counterparts of coronal mass ejections (ICMEs) are the leading driver of severe space weather. Their morphological evolution in interplanetary space and the prediction of their arrival time at Earth are the ultimate focus of space weather studies, because of their scientific and technological effects. Several investigations in the last couple of decades have assumed that ICMEs have a circular cross-section. Moreover, various models have also been developed to understand the morphology of ICMEs based on their deformed cross-section. In fact, simulation studies have suggested that the initial circular cross-section flattens significantly during their propagation in the solar wind and this is referred to as 'pancaking'. However, an observational verification of this phenmenon is still pending and it will eventually be the primary concern of several morphological models. Here, we report the first unambiguous observational evidence of extreme flattening of the cross-section of ICMEs, similar to pancaking, based on *in situ* measurements of 30 ICME events. In fact, we conclude that the cross-section of ICME flux ropes transformed into a two-dimensional planar magnetic structure. Such a deformed morphological feature not only alters the prediction of their arrival time but also has significant implications in solar-terrestrial physics, the energy budget of the heliosphere, charged particle energization, turbulence dissipation and enhanced geo-effectiveness, etc.

Key words: magnetic fields – plasmas – Sun: coronal mass ejections (CMEs) – Sun: heliosphere – solar-terrestrial relations – solar wind.

1 INTRODUCTION

Coronal mass ejections (CMEs) are one of the most violent forms of solar activity, in which huge amounts of plasma with accompanying magnetic field erupt from the solar corona and propagate into the heliosphere (Hudson, Bougeret & Burkepile 2006; Howard 2011; Owens, Lockwood & Barnard 2017). When their speed exceeds the ambient solar wind, they form a shock wave and sheath region (Kilpua, Koskinen & Pulkkinen 2017). CMEs and their sheath region are the major drivers of extreme space weather conditions near to Earth, and they can affect communication and navigation, overload power grids, cause rapid corrosion of pipelines, alter weather patterns, and cause radiation hazards for astronauts and high-altitude travellers (Schrijver & Siscoe 2010; Eastwood et al. 2017). CMEs have the potential to cause considerable damage to the global economy (Eastwood et al. 2017; Oughton et al. 2017). Thus, CMEs are important scientifically and technologically in space weather studies (Schrijver & Siscoe 2010; Cannon et al. 2013).

In the last few decades, space and ground-based observations, with the help of various modelling efforts, have significantly improved our understanding of CMEs. Their morphological and kinematic evolution in the heliosphere is the primary focus of these studies (Burlaga 1988; Lepping, Jones & Burlaga 1990; Hu & Sonnerup 2001; Wang et al. 2016; Manchester et al. 2017). Initially, the Large Angle and Spectrometric Coronagraph (LASCO) Experiment (Krall et al. 2001) detected three-part CMEs that indicate the existence of a flux rope structure. Furthermore, CMEs have been observed beyond coronographs and have been remotely sensed using interplanetary scintillation (Manoharan 2006); however, this method is affected by relatively poor temporal and spatial resolution. Observations from the heliospheric imager (HI) instrument onboard *Coriolis* and the *STEREO* satellite (Eyles et al. 2003, 2009; Kaiser et al. 2008) and coordinated efforts (Möstl et al. 2009; Liu et al. 2010) between imaging and *in situ* observations have tracked CMEs in our Solar system (Davies et al. 2009; Rouillard et al. 2009). However, the three-dimensional configuration of CMEs remains ambiguous.

The *in situ* measurments are often thought as a one-line crossing of spacecraft along the radial flow through three dimensional configuration of interplanetary CMEs (ICMEs). Therefore, *in situ*

★ E-mail: raghavanil1984@gmail.com

measurements often exhibit large event-to-event variability (Lepping et al. 2006; Zurbuchen & Richardson 2006). A significant part of our understanding of the morphology of ICMEs has come from studies of flux rope models. Initially, it was believed that idealized flux ropes often have a circular cross-section (Chen et al. 1997; Thernisien, Howard & Vourlidas 2006), which is further supported by various fitting models, such as the Lundquist model and the Gold–Hoyle model (Goldstein 1983; Burlaga 1988; Lepping et al. 1990; Hidalgo 2003; Wang et al. 2016). Hu & Sonnerup (2002) have used the Grad–Shafranov (GS) technique to study two-dimensional flux rope geometry and they have corroborated that most flux ropes have a circular cross-section at 1 au. However, observational studies suggest expansion and deflection of the ICMEs even though both CMEs and the ambient solar wind propagate radially away from the Sun (Berdichevsky, Lepping & Farrugia 2003; Wang et al. 2004; Wang, Du & Richardson 2005; Jian et al. 2006; Kilpua et al. 2009; Gulisano et al. 2010; Isavnin, Vourlidas & Kilpua 2013, 2014). Their anisotropic expansion may lead to the distortion of the initially circular cross-section geometry into a non-circular shape (Savani et al. 2010). A few studies also suggest a stretching and flattening of the shape as it propagates radially away from the Sun (Riley & Crooker 2004; Owens, Merkin & Riley 2006; Savani et al. 2011a,b). Therefore, non-circular cross-section (Vandas & Romashets 2003; Démoulin & Dasso 2009) or non-force-free models (Mulligan & Russell 2001; Hidalgo & Nieves-Chinchilla 2012; Wang et al. 2015, 2016) have also been developed to understand the more precise geometric information of the flux rope.

The above studies directly imply a significant deviation from a self-similar expansion of ICME flux ropes. In fact, numerical simulations have been utilized as a primary tool to investigate the propagation of ICMEs, in order to bridge the link between the evolutionary changes and the CME morphology. The accuracy of these heliospheric models has been continuously improving, but their complexity has been perpetually increasing (Riley, Linker & Mikić 2001; Manchester et al. 2004; Odstrčil, Riley & Zhao 2004; Kataoka et al. 2009; Nakamizo et al. 2009; Shiota et al. 2010; Feng 2020). These simulations are regularly tested and compared with observations. They are further employed to study various properties that may affect the morphology, such as the deceleration processes of ICMEs, their interactions with the fast and slow ambient solar wind and the interactions of multiple ICMEs (Lugaz, Manchester & Gombosi 2005). These simulation studies suggest that flux ropes that have circular cross-sections close to the Sun evolve into flattened objects (i.e. elliptical with a curved semimajor axis) during propagation, which is referred to as 'pancaking' (Riley & Crooker 2004; Savani et al. 2011a, b). However, direct observational evidence is not only elusive to date but also a matter of contention with the assumption that CMEs have a non-radial cross-section.

Recently, various studies have reported that the ICME sheath region transforms to a two-dimensional (2D) planar magnetic structure (PMS). This transformation is possibly caused by high compression or a draping of plasma around the ICME ejecta (Kataoka et al. 2005; Shaikh et al. 2018). The interaction of ICMEs with other ICMEs, with co-rotating interaction regions or with preceding slow or following fast solar wind could compress the ICME flux rope. Thus, we would expect a deformed cross-section in the *in situ* measurements. Therefore, the reported technique for identification of the PMS is implemented to study the morphological evolution of the cross-section of ICMEs observed by the *Advanced Composition Explorer* (*ACE*) spacecraft. Here, we list a total of 30 ICME flux ropes from the Richardson–Cane ICME list available at http://www.srl.caltech.edu/ACE/ASC/DATA/level3/icmetable2.htm, which qualifies PMS characteristics (see Table A1 in the Appendix, as only one event is explicitly discussed here). The study has used *in situ* interplanetary data of 64-s resolution from the *ACE* data base available at ftp://cdaweb.gsfc.nasa.gov/pub/data/ace/.

2 TYPICAL EVENT AND OBSERVATION

The selected ICME crossed the *ACE* spacecraft on 2003 November 20. The temporal variations of the interplanetary magnetic field (IMF) and plasma characteristics for the selected ICME are shown in Fig. 1. The recognition of the shock front is reflected in the interplanetary data as a sudden sharp enhancement in the IMF $B_{\rm mag}$, solar wind speed $V_{\rm p}$, proton temperature T and proton density $N_{\rm p}$ (see the first vertical black dashed line). The shock front is followed by high $N_{\rm p}$, T, $V_{\rm p}$ and plasma beta β, large fluctuations in the IMF vector components ($B_{\rm comp}$), identified as the ICME shock sheath (Kilpua et al. 2017; Shaikh, Raghav & Bhaskar 2017). The shock sheath is followed by the least fluctuations in $B_{\rm mag}$ and $B_{\rm comp}$, by a slow variation in θ and ϕ, by a slow steady trend in $V_{\rm p}$ and low β, indicating the transit of ICME flux rope (Zurbuchen & Richardson 2006). A different shades of colour are used to show ICME substructures (i.e. the shock sheath and flux rope; see Fig. 1).

In the literature, the following criteria have been utilized to identify PMS (Palmerio, Kilpua & Savani 2016; Shaikh et al. 2018): (i) a wide azimuth angle spread $0^\circ < \phi < 360^\circ$; (ii) good planarity, that is, $|B_n|/B \leq 0.2$, where B is the IMF magnitude and B_n is the normal IMF to the PMS plane (i.e. $B_n = \boldsymbol{B} \cdot \boldsymbol{n}$); (iii) good efficiency, $R = \lambda_2/\lambda_3 \geq 3$ (Nakagawa, Nishida & Saito 1989; Nakagawa 1993; Neugebauer, Clay & Gosling 1993; Jones, Balogh & Horbury 1999; Jones & Balogh 2001; Shaikh et al. 2018). Here, λ_1, λ_2 and λ_3 are eigenvalues and $\hat{n}$ is the normal direction of PMS calculated after minimum and maximum variance analysis (MVA; Sonnerup & Scheible 1998). If $B_n = 0$, the region is said to be a perfect plane, and then a low value of $|B_n|/B$ indicates good planarity (Neugebauer et al. 1993; Palmerio et al. 2016).

Fig. 2 shows a distribution of θ (elevation angle) and ϕ (azimuth angle) during flux rope transit. It is consistent with the expected distribution for PMS. The distribution follows a wave-like pattern (see the fitted model curve in Fig. 2). The studied ICME flux rope has $|B_n|/\langle B\rangle = 0.15$ and $\lambda_2/\lambda_3 = 14.35$, which confirms the existence of PMS structure (Nakagawa et al. 1989; Neugebauer et al. 1993; Jones et al. 1999; Shaikh et al. 2018). The normal vector to the PMS plane is $\boldsymbol{n} = (0.990, 0.098, -0.099)$. The PMS is inclined to the ecliptic plane with an angle of $\theta_{\rm max} = 84.^\circ89$. Moreover, at $\theta = 0$, the PMS plane intersects $\sim\phi = 82.^\circ72$ and $264.^\circ80$. This implies that the PMS plane includes an Archimedean spiral direction (Nakagawa et al. 1989; Nakagawa 1993; Jones et al. 1999; Kilpua et al. 2017). All the listed ICME flux ropes exhibit plasma features that are consistent with the standard PMS characteristics. Thus, we unambiguously conclude that the flux rope cross-section flattened to such extent that the *in situ* measurements (spacecraft transit in one line) interpreted them as PMS.

3 DISCUSSION AND IMPLICATIONS

The recent simulation studies of the evolution of CMEs simulated the continuous flattening of their cross-sections as they propagate further into the heliosphere, called pancaking (Riley & Crooker 2004). Russell & Mulligan (2002) suggested that a cross-flow diameter of the flux rope may be of the order of four times the

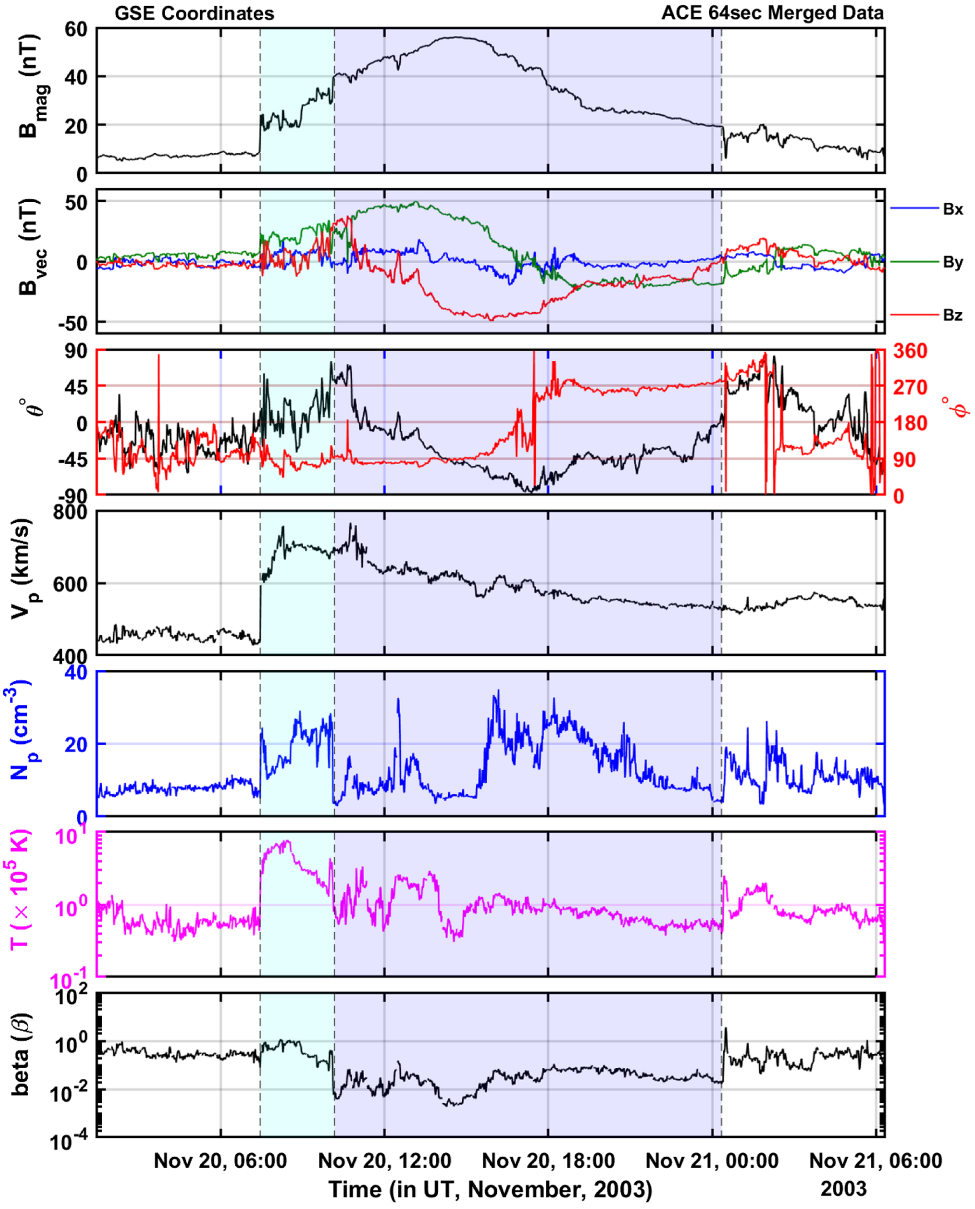

Figure 1. The *ACE* spacecraft observed an ICME crossing the Earth on 2003 November 20. There are seven subpanels. The top two panels show the temporal variations of the IMF $B_{\rm mag}$ and $B_{\rm vec}$ (i.e. B_X, B_Y and B_Z). The third panel represents the azimuth (ϕ) and elevation (θ) angles of the IMF vector. The fourth panel represents the time evolution of solar wind speed ($V_{\rm p}$). The fifth panel shows plasma density ($N_{\rm p}$). The sixth and seventh panels give the temporal evolution of temperature ($T_{\rm p}$) and plasma beta (β), respectively. The first vertical black dashed line denotes the shock onset time. The shock sheath and magnetic cloud (MC) regions are separated by different coloured shading.

radial thickness of CMEs, based on indirect evidence. A model-based study by Liu et al. (2006) found a highly flattened and curved cross-section with a minimum aspect ratio of 6 : 1. Moreover, Savani et al. (2011a) quantified the cross-section of flux rope using remote observational data and a mathematical parameter called the aspect ratio (i.e. the ratio of the semiminor axis to semimajor axis) based on geometric arguments. They concluded that the aspect ratio of CMEs converges to a fixed value (i.e. $1:5 \pm 1$) if the ratio between the expansion velocity and bulk flow remains constant. This means that the CME morphology can become scale-invariant as it propagates out into the heliosphere.

In the literature, the deformation of the flux rope was interpreted based on the expansion velocity. The decrease in the expansion velocity leads to an increase in the aspect ratio, which further implies an increasingly more flattened cross-section. The solar wind expands only in non-radial directions, whereas an ICME often expands in all directions. This implies that the plasma pressure in an ICME decreases faster than the solar wind. The lower internal pressure weakens the ICME expansion, further leading to flattening the cross-section (Savani et al. 2011a, b). This means that the dynamic interaction of ambient solar wind changes the CME morphology. In fact, the location of the slow and fast solar wind boundaries to the rear of the CME at the time of launch can have a significant effect on changing the cross-sectional shape of the CME (Odstrčil & Pizzo 1999; Savani et al. 2010). In addition to this, CME–CME and CME–corotating interaction region interactions may also influence CME morphology. The *in situ* signature of such a flattened cross-section is, so far, missing. Up to a certain extent,

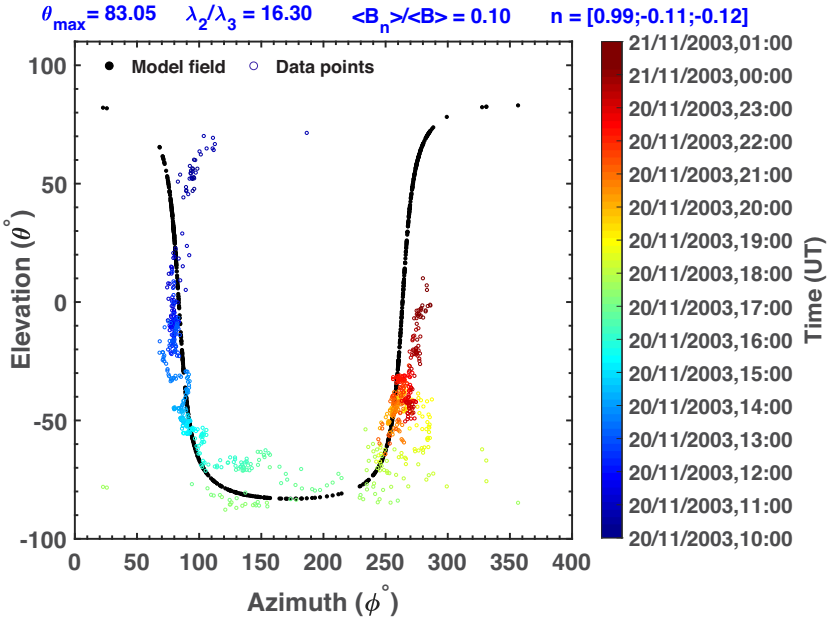

Figure 2. Distribution of azimuth (ϕ) versus elevation (θ) angle of the IMF in geocentric solar ecliptic coordinates. Note that λ_2/λ_3, $\langle B_n \rangle / B$ and n give information about the planarity, efficiency and normal direction of the PMS. $\theta_{\max}$ is the inclination of the PMS plane with respect to the ecliptic plane. When IMF vectors $\boldsymbol{B} = (B_x, B_y, B_z) \equiv (B\cos\theta\cos\phi, B\cos\theta\sin\phi, B\sin\theta)$ are parallel to a plane whose normal is $\boldsymbol{n} \equiv (n_x, n_y, n_z)$, the relation between ϕ and θ is given as $n_x \cos\theta\cos\phi + n_y \cos\theta\sin\phi + n_z \sin\theta = 0$. The above curve fitting (see the black dotted curve) to the measured (coloured dots) ϕ and θ indicates the presence of PMS.

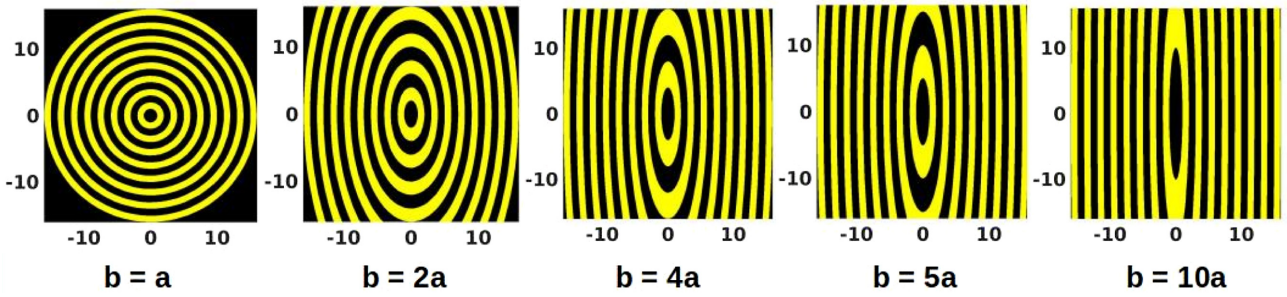

Figure 3. The flattened cross-section of the flux rope is estimated using different ratios of semimajor to semiminor axes.

these measurements are supported by the identification of PMS in CME-driven sheaths. However, no arguments have yet been made concerning CME flux ropes.

In the present study, we have assumed that higher aspect ratios are possible and therefore their effect on the cross-section is shown in Fig. 3. As the aspect ratio increases, the cross-section flattens drastically (see Fig. 3, left to right; i.e. $b = a$ to $b = 10a$). If such a highly flattened cross-section of flux rope evolved and crossed over the spacecraft, then it provides time-series plasma measurements in a one-dimensional cut, which can be interpreted as 2D PMS. This implies that the identified PMS (modified flux ropes) are nothing but clear observational evidence of highly flattened ICMEs that demonstrate features similar to pancakes. However, the extent of flattening is beyond the scope of this study.

In general, two major physical mechanisms are proposed for the generation of PMS within the ICME sheath region. The first process is the draping of plasma around the flux rope, aligned with magnetic field lines of the solar wind parallel to their surface (Jones et al. 2002; Palmerio et al. 2016). The second process is the high compression in the downstream region of solar wind aligned with the pre-existing microstructures and discontinuities parallel to the shock plane (Farrugia et al. 1990; Nakagawa 1993; Neugebauer et al. 1993; Palmerio et al. 2016; Shaikh et al. 2018). The high density in the PMS may be the result of some additional mechanism (e.g. a piled-up compression region forms due to lateral expansion of the CME), which can affect the ion profiles of the accelerated solar energetic particles (Das et al. 2011). The high proton density, which is not expected in regular flux rope, is also clearly visible in our case (see Fig. 1). Kataoka et el. (2005) suggest that PMS is absent for $\beta < 0.05$ (Kataoka et al. 2005) for sheath regions. However, our study also identifies PMS for flux ropes that have lower β values. This implies that the concentric cylindrical surfaces of the flux ropes (with a circular cross-section) are crushed to elliptical surface layers under high compression caused by ICME interactions and form the observed PMS. Further investigation is needed to understand the origin of PMS in stable magnetic structures.

In addition to this, Intriligator, Rees & Horbury (2008) performed a multi-spacecraft study of PMS characteristics from 1 to 93 au. They suggest that the features of PMS planarity improve significantly as it propagates farther out in the heliosphere (Intriligator

et al. 2008). This implies that the flattening of the flux rope cross-section (planarity of identified PMS as flux ropes) may increase as it moves away from the Sun, which is consistent with the assumption used in various simulation studies. The specific 2D PMS of flux ropes in solar wind will definitely affect the drag coefficient, which leads to a different prediction of the arrival time of CMEs at Earth. Owens & Crooker (2006) suggested the importance of ICME morphology to estimate total helicity and the heliospheric flux budget. Besides this, the evolution of space plasma as 2D slab-like structure (Zank et al. 2018) or with Alfvénic nature (Raghav & Kule 2018a, b; Raghav & Shaikh 2018; Raghav et al. 2018; Raghav, Choraghe & Shaikh 2019; Shaikh, Raghav & Vichare 2019) is important for the plasma fluctuations and energy dissipation, plasma turbulence and particle energization. The PMS identified in sheath regions is causing great geomagnetic storms (Kataoka et al. 2015; Palmerio et al. 2016), as well as a decrease in the cosmic ray flux observed on the Earth's surface (Shaikh et al. 2018), that is, Forbush decrease phenomena (Raghav et al. 2014, 2017; Bhaskar et al. 2016). The results of this study (i.e. the identification of flux ropes transformed to PMS) will definitely have a significant role in the aforementioned physical processes involved in solar-terrestrial physics, the energy budget of the heliosphere, charged particle energization, turbulence dissipation, enhanced geo-effectiveness, etc. However, a detailed investigation of each case is needed in the future.

ACKNOWLEDGEMENTS

We thank the ACE MAG and SWEPAM instrument team and ACE science Center for providing the ACE data.

REFERENCES

Berdichevsky D., Lepping R., Farrugia C., 2003, Phys. Rev. E, 67, 036405
Bhaskar A., Vichare G., Arunbabu K., Raghav A., 2016, Ap&SS, 361, 242
Burlaga L., 1988, J. Geophys. Res.: Space Phys., 93, 7217
Cannon P. et al., 2013, Extreme Space Weather: Impacts on Engineered Systems and Infrastructure. Royal Academy of Engineering, London
Chen J. et al., 1997, ApJ, 490, L191
Das I., Opher M., Evans R., Loesch C., Gombosi T. I., 2011, ApJ, 729, 112
Davies J. et al., 2009, Geophys. Res. Lett., 36, L02102
Démoulin P., Dasso S., 2009, A&A, 498, 551
Eastwood J. et al., 2017, Risk Analysis, 37, 206
Eyles C. et al., 2003, Solar Phys., 217, 319
Eyles C. et al., 2009, Solar Phys., 254, 387
Farrugia C., Dunlop M., Geurts F., Balogh A., Southwood D., Bryant D., Neugebauer M., Etemadi A., 1990, Geophys. Res. Lett., 17, 1025
Feng X., 2020, Magnetohydrodynamic Modeling of the Solar Corona and Heliosphere. Springer, Berlin, p. 1
Goldstein H., 1983, in JPL Solar Wind Five. NASA JPL, Pasadena, CA, p. 731
Gulisano A. M., Démoulin P., Dasso S., Ruiz M. E., Marsch E., 2010, A&A, 509, A39
Hidalgo M., 2003, J. Geophys. Res.: Space Phys., 108, 1320
Hidalgo M., Nieves-Chinchilla T., 2012, ApJ, 748, 109
Howard T., 2011, Coronal Mass Ejections: An Introduction, Vol. 376. Springer , Berlin
Hu Q., Sonnerup B. U., 2001, Geophys. Res. Lett., 28, 467
Hu Q., Sonnerup B. U., 2002, J. Geophys. Res.: Space Phys., 107, 1142
Hudson H., Bougeret J.-L., Burkepile J., 2006, in Coronal Mass Ejections. Springer, Berlin, p. 13
Intriligator D. S., Rees A., Horbury T. S., 2008, J. Geophys. Res.: Space Phys., 113, A05102
Isavnin A., Vourlidas A., Kilpua E., 2013, Solar Phys., 284, 203
Isavnin A., Vourlidas A., Kilpua E. K., 2014, Solar Phys., 289, 2141
Jian L., Russell C., Luhmann J., Skoug R., 2006, Solar Phys., 239, 393
Jones G. H., Balogh A., 2001, in Marsden R. G., ed., The 3-D Heliosphere at Solar Maximum. Springer, Berlin, p. 165
Jones G., Balogh A., Horbury T., 1999, Geophys. Res. Lett., 26, 13
Jones G., Rees A., Balogh A., Forsyth R., 2002, Geophys. Res. Lett., 29, 1520
Kaiser M. L., Kucera T., Davila J., Cyr O. S., Guhathakurta M., Christian E., 2008, Space Sci. Rev., 136, 5
Kataoka R., Watari S., Shimada N., Shimazu H., Marubashi K., 2005, Geophys. Res. Lett., 32, L12103
Kataoka R., Ebisuzaki T., Kusano K., Shiota D., Inoue S., Yamamoto T., Tokumaru M., 2009, J. Geophys. Res.: Space Phys., 114, A10102
Kataoka R., Shiota D., Kilpua E., Keika K., 2015, Geophys. Res. Lett., 42, 5155
Kilpua E. et al., 2009, Ann. Geophys.: Atmospheres, Hydrospheres and Space Sciences, 27, 4491
Kilpua E., Koskinen H. E., Pulkkinen T. I., 2017, Living Reviews in Solar Physics, 14, 5
Krall J., Chen J., Duffin R., Howard R., Thompson B., 2001, ApJ, 562, 1045
Lepping R., Jones J., Burlaga L., 1990, J. Geophys. Res., 95, 11957
Lepping R., Berdichevsky D., Wu C.-C., Szabo A., Narock T., Mariani F., Lazarus A., Quivers A., 2006, Ann. Geophys., 24, 215
Liu Y., Richardson J., Belcher J., Wang C., Hu Q., Kasper J., 2006, J. Geophys. Res.: Space Phys., 111, A12S03
Liu Y., Thernisien A., Luhmann J. G., Vourlidas A., Davies J. A., Lin R. P., Bale S. D., 2010, ApJ, 722, 1762
Lugaz N., Manchester W. IV, Gombosi T., 2005, ApJ, 634, 651
Manchester W. B. IV, Gombosi T. I., Roussev I., De Zeeuw D. L., Sokolov I., Powell K. G., Tóth G., Opher M., 2004, J. Geophys. Res.: Space Phys., 109, A01102
Manchester W., Kilpua E. K., Liu Y. D., Lugaz N., Riley P., Török T., Vršnak B., 2017, Space Sci. Rev., 212, 1159
Manoharan P., 2006, Solar Phys., 235, 345
Möstl C., Farrugia C. J., Temmer M., Miklenic C., Veronig A. M., Galvin A. B., Leitner M., Biernat H. K., 2009, ApJ, 705, L180
Mulligan T., Russell C., 2001, J. Geophys. Res.: Space Phys., 106, 10581
Nakagawa T., 1993, Solar Phys., 147, 169
Nakagawa T., Nishida A., Saito T., 1989, J. Geophys. Res.: Space Phys., 94, 11761
Nakamizo A., Tanaka T., Kubo Y., Kamei S., Shimazu H., Shinagawa H., 2009, J. Geophys. Res.: Space Phys., 114, A07109
Neugebauer M., Clay D., Gosling J., 1993, J. Geophys. Res.: Space Phys., 98, 9383
Odstrčil D., Pizzo V., 1999, J. Geophys. Res.: Space Phys., 104, 493
Odstrčil D., Riley P., Zhao X., 2004, J. Geophys. Res.: Space Phys., 109, A02116
Oughton E. J., Skelton A., Horne R. B., Thomson A. W., Gaunt C. T., 2017, Space Weather, 15, 65
Owens M. J., Crooker N., 2006, J.Geophys. Res.: Space Phys., 111, A10104
Owens M. J., Merkin V., Riley P., 2006, J. Geophys. Res.: Space Phys., 111, A03104
Owens M., Lockwood M., Barnard L., 2017, Scientific Reports, 7, 4152
Palmerio E., Kilpua E. K., Savani N. P., 2016, Ann. Geophys., 34, 313
Raghav A. N., Kule A., 2018a, MNRAS, 476, L6
Raghav A. N., Kule A., 2018b, MNRAS, 480, L6
Raghav A. N., Shaikh Z. I., 2018, preprint (arXiv:1810.06004)
Raghav A., Bhaskar A., Lotekar A., Vichare G., Yadav V., 2014, J. Cosmol. Astropart. Phys., 2014, 074
Raghav A., Shaikh Z., Bhaskar A., Datar G., Vichare G., 2017, Solar Phys., 292, 99
Raghav A. N., Kule A., Bhaskar A., Mishra W., Vichare G., Surve S., 2018, ApJ, 860, 26
Raghav A. N., Choraghe K., Shaikh Z. I., 2019, MNRAS, 488, 910
Riley P., Crooker N., 2004, ApJ, 600, 1035
Riley P., Linker J., Mikić Z., 2001, J. Geophys. Res.: Space Phys., 106, 15889
Rouillard A. et al., 2009, J. Geophys. Res.: Space Phys., 114, A07106

Russell C., Mulligan T., 2002, Adv. Space Res., 29, 301
Savani N., Owens M. J., Rouillard A., Forsyth R., Davies J., 2010, ApJ, 714, L128
Savani N., Owens M. J., Rouillard A., Forsyth R., Kusano K., Shiota D., Kataoka R., 2011a, ApJ, 731, 109
Savani N. et al., 2011b, ApJ, 732, 117
Schrijver C. J., Siscoe G. L., 2010, Heliophysics: Space Storms and Radiation: Causes and Effects. Cambridge Univ. Press, Cambridge
Shaikh Z., Raghav A., Bhaskar A., 2017, ApJ, 844, 121
Shaikh Z. I., Raghav A. N., Vichare G., Bhaskar A., Mishra W., 2018, ApJ, 866, 118
Shaikh Z. I., Raghav A., Vichare G., 2019, MNRAS, 490, 1638
Shiota D., Kusano K., Miyoshi T., Shibata K., 2010, ApJ, 718, 1305
Sonnerup B. U., Scheible M., 1998, in Paschmann G., Daly P. W., eds, ISSI Scientific Report SR-001, Analysis Methods for Multi-Spacecraft Data. ISSI, Bern, Switzerland, p. 185
Thernisien A., Howard R., Vourlidas A., 2006, ApJ, 652, 763
Vandas M., Romashets E., 2003, A&A, 398, 801
Wang C., Du D., Richardson J., 2005, J. Geophys. Res.: Space Phys., 110, A10107
Wang Y., Shen C., Wang S., Ye P., 2004, Solar Phys., 222, 329
Wang Y., Zhou Z., Shen C., Liu R., Wang S., 2015, J. Geophys. Res.: Space Phys., 120, 1543
Wang Y., Zhuang B., Hu Q., Liu R., Shen C., Chi Y., 2016, J. Geophys. Res.: Space Phys., 121, 9316
Zank G., Adhikari L., Hunana P., Tiwari S., Moore R., Shiota D., Bruno R., Telloni D., 2018, ApJ, 854, 32
Zurbuchen T. H., Richardson I. G., 2006, in Kunow H. et al., eds, Coronal Mass Ejections. Springer, Berlin, p. 31

APPENDIX

Table A1. List of ICME flux rope events transformed to PMS.

MC start	MC end	nx	ny	nz	λ_1	λ_2	λ_3	λ_1/λ_2	λ_2/λ_3	B_{avg}	V_{avg}	β_{avg}	B_n/B	θ_{max}
1998-06-02 10:00	1998-06-02 18:00	−0.83	0.47	−0.30	24.20	7.81	0.74	3.10	10.50	9.80	399.79	0.15	0.13	72.43
1998-06-24 15:59	1998-06-25 23:00	−0.70	−0.63	−0.33	77.12	24.29	3.76	3.17	6.47	13.20	457.61	0.11	0.13	70.63
1998-11-07 22:00	1998-11-09 01:00	−0.96	0.18	−0.23	267.31	127.84	10.17	2.09	12.56	23.86	534.00	0.08	0.10	76.65
1999-12-12 18:59	1999-12-13 15:59	−0.97	0.09	−0.21	48.24	12.22	1.66	3.95	7.37	11.78	538.79	0.11	0.18	52.58
2000-06-04 22:00	2000-06-06 22:00	−0.75	−0.66	0.06	50.03	26.67	4.24	1.88	6.28	8.92	454.59	0.33	0.18	86.79
2000-08-12 04:59	2000-08-13 22:00	−0.97	−0.07	−0.25	226.81	98.78	9.32	2.30	10.60	17.37	570.04	0.04	0.14	75.32
2000-10-28 21:00	2000-10-29 22:00	−0.87	−0.26	0.42	43.67	7.67	1.16	5.70	6.62	14.27	384.27	0.05	0.19	52.01
2001-04-21 23:00	2001-04-23 02:59	−0.98	0.17	−0.11	41.57	21.11	2.51	1.97	8.39	11.44	356.52	0.09	0.14	83.55
2001-10-31 19:59	2001-11-02 11:59	−0.99	0.12	−0.02	68.79	11.46	2.19	6.00	5.24	10.58	336.00	0.07	0.14	88.84
2001-12-29 23:59	2001-12-30 18:00	0.87	−0.11	−0.47	163.31	63.99	2.92	2.55	21.90	16.69	397.36	0.16	0.11	61.72
2002-03-24 12:00	2002-03-25 20:00	0.89	0.16	−0.42	50.95	17.30	1.67	2.94	10.34	15.59	433.94	0.04	0.07	65.20
2002-05-11 15:00	2002-05-12 00:00	−0.95	0.19	−0.23	64.42	26.99	7.22	2.39	3.74	13.11	426.13	0.47	0.17	76.64
2003-05-30 01:59	2003-05-30 16:00	0.86	0.32	−0.40	120.50	68.17	22.47	1.77	3.03	20.65	601.82	0.21	0.19	66.37
2003-11-20 10:10	2003-11-21 00:20	0.99	−0.11	−0.12	721.29	370.67	22.75	1.95	16.30	38.14	590.59	0.04	0.10	83.05
2004-07-27 01:59	2004-07-27 21:59	−0.92	−0.22	0.33	103.66	82.63	7.78	1.25	10.63	17.99	875.72	0.30	0.13	70.57
2004-09-18 12:00	2004-09-20 00:00	−0.80	−0.42	0.43	23.13	4.75	1.45	4.87	3.28	5.94	396.57	0.14	0.18	64.54
2005-01-21 19:00	2005-01-22 16:59	0.14	0.51	−0.85	117.49	48.78	15.60	2.41	3.13	17.67	815.61	0.13	0.15	31.06
2005-06-12 15:00	2005-06-13 12:59	−0.89	−0.39	−0.25	47.69	10.64	1.72	4.48	6.17	13.51	471.02	0.08	0.07	74.62
2005-06-15 04:59	2005-06-16 08:59	0.76	0.17	−0.63	53.33	18.62	3.83	2.86	4.86	9.21	479.75	0.11	0.17	50.81
2005-07-10 10:00	2005-07-12 03:59	−0.78	−0.06	0.62	63.77	23.57	7.27	2.71	3.24	11.80	425.00	0.12	0.19	35.17
2005-08-24 14:00	2005-08-24 22:59	−0.92	−0.26	−0.30	83.78	60.09	6.93	1.39	8.67	19.08	658.80	0.20	0.14	71.64
2006-11-29 05:00	2006-11-30 10:00	0.86	−0.22	−0.45	61.16	37.60	1.68	1.63	22.40	11.81	419.14	0.05	0.17	63.09
2013-04-14 16:59	2013-04-15 23:00	0.86	−0.36	−0.36	21.51	8.83	1.55	2.44	5.69	9.47	411.63	0.01	0.10	68.71
2013-07-13 04:59	2013-07-14 23:59	−0.96	−0.28	−0.09	72.02	26.64	2.47	2.70	10.80	12.28	403.79	0.02	0.10	84.07
2013-10-02 22:59	2013-10-03 22:00	0.58	−0.50	−0.64	13.30	4.41	0.66	3.02	6.68	7.29	461.34	0.02	0.18	49.83
2014-04-21 07:00	2014-04-22 08:59	−0.29	0.93	0.24	24.72	3.40	0.85	7.28	3.99	5.50	540.19	0.07	0.19	76.07
2014-08-19 15:59	2014-08-21 04:59	0.92	−0.04	−0.38	127.95	102.29	3.14	1.25	32.57	16.55	360.77	0.04	0.11	67.75
2015-01-07 06:59	2015-01-07 20:00	0.66	−0.70	0.26	136.78	35.12	4.70	3.89	7.48	18.55	442.87	0.03	0.14	74.67
2015-05-06 12:00	2015-05-07 20:59	−0.92	0.09	−0.39	52.67	26.15	2.08	2.01	12.55	11.68	418.07	0.09	0.13	67.24
2016-10-13 06:00	2016-10-14 15:59	0.97	0.00	−0.24	156.64	55.42	3.66	2.83	15.15	19.43	386.01	0.02	0.11	75.04

This paper has been typeset from a TEX/LATEX file prepared by the author.